This is the accepted manuscript made available via CHORUS. The article has been published as:

# Short- and medium-range order in Zr_{80}Pt_{20} liquids

N. A. Mauro, V. Wessels, J. C. Bendert, S. Klein, A. K. Gangopadhyay, M. J. Kramer, S. G. Hao, G. E. Rustan, A. Kreyssig, A. I. Goldman, and K. F. Kelton

Phys. Rev. B **83**, 184109 — Published 18 May 2011

DOI: 10.1103/PhysRevB.83.184109

# Short and Medium Range Order in $Zr_{80}Pt_{20}$ Liquids

N. A Mauro[1], V. Wessels[2], J. C. Bendert[1], S. Klein[3,4], A. K. Gangopadhyay[1], M. J. Kramer[5], S. G. Hao[6], G. E. Rustan[6], A. Kreyssig[6], A. I. Goldman[6], K. F. Kelton[1]

[1]*Department of Physics, Center for Materials Innovation, Washington University, St. Louis, MO 63130-4899*
[2]*ETH Zurich, Dept. of Materials, Zurich, Switzerland*
[3]*Institut für Materialphysik im Weltraum, Deutsches Zentrum für Luft- und Raumfahrt (DLR), 51170 Köln, Germany*
[4]*Institut für Festkörperphysik, Ruhr-Universität Bochum, 44780 Bochum, Germany*
[5]*Ames Laboratory and Department of Materials Science and Engineering, Iowa State University, Ames IA 50011*
[6]*Department of Physics and Astronomy, Iowa State University, Ames, IA 50011*

## *Abstract*

The atomic structures in equilibrium and supercooled liquids of $Zr_{80}Pt_{20}$ were determined as a function of temperature by *in-situ* high-energy synchrotron diffraction studies of the levitated liquids (containerless processing) using the beamline electrostatic levitation (BESL) technique. The presence of a pronounced pre-peak at $q \sim 1.7$ Å$^{-1}$ in the static structure factor indicates medium range order (MRO) in the liquid. The position and intensity of the pre-peak remain constant with cooling, indicating that the MRO is already present in the liquid above its melting temperature. An analysis of the liquid atomic structures obtained using the Reverse Monte Carlo (RMC) method utilizing both the structure factor, *S(q)*, from x-ray diffraction experiments and the partial pair-correlation functions from *ab initio* molecular dynamics (MD) simulations show that the pre-peak arises from a Pt-Pt correlation that can be indentified with icosahedral short-range order around the Pt atoms. The local atomic ordering is dominated by icosahedral-like structures, raising the nucleation barrier between the liquid and these phases, thus assisting glass formation.

## I. Introduction

It is well known that Zr-based metallic glasses tend to have a high glass forming ability (GFA).[1, 2] Some are bulk metallic glasses (BMG's), i.e. glasses with a critical casting thickness of 1 mm or greater. Icosahedral quasicrystal phases (i-phases) are frequently found in crystallized Zr-based BMG's,[3-7] suggesting that these amorphous structures have a high degree of icosahedral short-range order (ISRO). This is supported by recent high-energy synchrotron X-ray diffraction studies of Zr/Ti-based liquids and glasses, which have linked supercooling and the glass transition to an increase in icosahedral and icosahedral-like local order.[8-10] More quantitative structural studies of BMG's, however, are hindered by their chemical complexity, often containing four or more components. Studies of simpler Zr-based binary alloys have been more successful, providing important

insights into the role of local atomic structures in dictating the transformation pathways and supercooling potential for a liquid.[11]

It has been reported that $Zr_{80}Pt_{20}$ can be quenched into the amorphous state by melt-spinning[12, 13] and that the X-ray diffraction patterns of the glassy ribbons show a pre-peak near 1.7 $Å^{-1}$.[14] Studies of $Zr_xPt_{100-x}$ ($73 \leq x \leq 77$) glasses[15] show that the intensity of the pre-peak increases with increasing Pt concentration, suggesting that it arises from Pt-Pt correlations. Pre-peaks, indicating some degree of medium-range order (MRO), have been observed previously in experimental[15-19] and theoretical[18, 20, 21] studies of metallic glasses and liquids. However, reports of MRO in metal-metal liquids are rare,[22,23] found primarily in metal-metalloid binary[24, 25] and Al-based binary and ternary[17, 26, 27] alloys. In this letter, we present the results from *in-situ* high-energy synchrotron X-ray diffraction studies of equilibrium and supercooled $Zr_{80}Pt_{20}$ liquids (eutectic composition) using the Beamline Electrostatic Levitation (BESL)[28] technique. These data show that the MRO is very stable, with the pre-peak present from 550°C above the liquidus temperature, $T_l$, in the equilibrium liquids to 200°C below $T_l$ in the supercooled liquid, the lowest temperature that could be studied before crystallization. Consistent with previous structural studies of melt-spun ribbons of the same composition, the MRO observed in the liquid is dominated by a Pt-Pt correlation. The new results presented here show that the MRO is already established well above the melting temperature and remains relatively unchanged over the 750°C temperature range studied. The Honeycutt Andersen (HA) and Voronoi polyhedra (VI) analyses of the atomic structures obtained by Reverse Monte Carlo (RMC) fits to the measured scattering data in a more limited temperature range show that the liquid is dominated by icosahedral and icosahedral-like local order, which increases modestly with supercooling. Further, the Voronoi polyhedra analysis shows that the dominant Pt-centered and Zr-centered clusters in the liquid are similar from those reported in the amorphous alloy and that the MRO established in the high-temperature liquid is dominated by a Pt-Pt correlation.

## II. Experimental

Master ingots (~1.0g) of $Zr_{80}Pt_{20}$ were prepared by arc-melting high purity elemental Zr (99.95% (including nominal Hf 3%)) and Pt (99.995%) on a water-cooled copper hearth in a high-purity Ar (99.999%) atmosphere. These ingots were crushed and small spherical samples (~2.5 mm) were prepared for supercooling and *in-situ* liquid structure studies at the Advanced Photon Source (Station 6-ID-D in the MUCAT Sector), using the Washington University Beamline Electrostatic Levitator (WU-BESL).[29] WU-BESL is a recently constructed facility that is optimized for diffraction studies of levitated (containerless) liquids under high vacuum; the design is a modified version of the prototype Electrostatic Levitation (ESL)[28] facilities at the NASA Marshall space flight center and the DLR (Cologne, Germany).[30]

Two optical pyrometers were used to measure the sample temperature over two ranges, 160-800°C and 600-2300°C, with a relative accuracy of better than 1% over the entire temperature range. To obtain maximum supercooling, the levitated samples were heated

in a high vacuum environment (~$10^{-7}$ torr) using a fiber coupled diode laser (980nm, 50W continuous maximum power output) to 300°C above the liquidus temperature, $T_l$, and subsequently free-cooled (radiation cooling with laser power off). Crystallization from the metastable liquid, marked by a sharp rise in temperature (recalescence), limited the lowest temperature of X-ray diffraction studies to 250°C below $T_l$. By controlling the laser power, it was also possible to make isothermal measurements at different temperatures. The mass loss during processing was negligible (< 0.2 %). Simultaneous non-contact density measurements were made using the shadow method[31, 32] with a Pixelink PL-B742U CCD camera and a 450 nm backlight. Video data were taken at a frame rate of 15 fps averaging of up to 300 frames at each isothermal step. The details of machine vision volume measurement algorithm are described elsewhere.[32] The relative precision of the density data was ~1.5% over the temperature range studied with an absolute accuracy of 3%.

High energy (E = 129 keV, $\lambda$ = 0.0969Å) diffraction studies of the liquids were made in a transmission geometry to high-q (15 $Å^{-1}$) using a GE Revolution 41-RT amorphous Si flat panel X-ray detector at a sampling rate of 1 Hz. Structure factors, $S(q)$, were derived from the scattering data, by first applying an appropriate gain map, masking bad pixels, and averaging images, subtracting the appropriate dark current and then correcting for oblique incidence, absorption, multiple scattering, fluorescence and Compton scattering contributions by using Fit2d[33] and PDFGetX2[34] analysis packages. Liquid diffraction patterns were obtained as a function of temperature by taking 20 second exposures per temperature step. The static structure factor was calculated using,

$$S(q) = \frac{I(q) - \sum_i^n a_i |f_i(q)|^2}{\left| \sum_i^n a_i f_i(q) \right|^2} + 1 \qquad (1)$$

where $I(q)$ is the measured diffraction intensity, $a_i$ is the atomic fraction of each element, and $f_i(q)$ is the $q$-dependent atomic form factor for each species. The sums are over all species and an isotropic and statistically homogeneous atomic distribution is assumed. This approximation is well justified in metallic liquids.

Atomic structures were obtained by Reverse Monte Carlo (RMC) fits to the measured X-ray static structure factors, $S(q)$ while constraining the simulation with partial pair distribution functions obtained from *ab initio* Molecular Dynamics (MD) simulations using the Vienna *ab initio* simulation package (VASP).[35-39] The system consisted of 100 atoms _80 atoms of Zr and 20 atoms of Pt_ in a cubic box with periodic boundary conditions, described more fully in Wang *et a.l*[40] The MD simulations provide partial pair correlation functions out to ~ 6 Å when none are experimentally available. The description and details of the constrained RMC (CRMC) technique can be found elsewhere.[41-43] For this study, random starting configurations of 5000 atoms with the appropriate stoichiometric composition were used, confined to a cubic box with dimensions appropriate to the measured density. The CRMC partial minimum distances were set nominally at 2.00Å for all atomic pairs, consistent with the measured total radial

distribution function, $g(r)$, and the MD partial pair correlation functions. The $g(r)$ data demonstrated that this minimum distance changed little relative to the position of the main peak over the temperature range studied. The SRO of the atomic structures obtained from the CRMC process was evaluated using both the Honeycutt and Andersen index[44] and Voronoi tessellation[45, 46] methods. A nearest-neighbor cutoff distance of nominally 4.08Å was used for these studies, again determined from the total *g(r)*.

## III. Results and Discussions

With cooling, the levitated liquid drops show a single recalescence near 978°C (197°C below the liquidus temperature). The diffraction data following that recalescence can be indexed to a phase mixture of $Zr_5Pt_3$ (hexagonal) and β-Zr, consistent with the equilibrium phase diagram for the eutectic liquid.[47] The measured liquid X-ray static structure factors determined from 1607°C, 432°C above the liquidus temperature ($T_l$ = 1175°C), down to the maximum supercooling of 197°C (T=978°C) are shown in Fig. 1. The $S(q)$ oscillates well around unity over the entire range of $q$ (Fig 1a.), indicating the high quality of the experimental data and that the appropriate correction were made for absorption, background and Compton scattering. The primary peak (Fig 1b.) sharpens, increases in magnitude, and shifts to lower scattering angle, reflecting an increasing density and a more ordered liquid with decreasing temperature. The shoulder on the second peak (Fig 1c.) becomes more pronounced with supercooling, which is frequently argued to indicate an increase in icosahedral and icosahedral-like order.[9] A pre-peak is observed at ~1.7 $Å^{-1}$ for all temperatures (Fig 1d.). The small variation of the pre-peak with cooling indicates that the atomic bonds associated with the MRO are strong compared to thermal energy. This pre-peak is of interest because it doesn't often emerge in X-ray scattering studies of liquids. To investigate atomic structures in the liquids, and in particular to gain insight into the chemical ordering constrained Reverse Monte Carlo fits were performed on the S(q) data at all temperatures.

*Figure 1 near here*

Convergence of the CRMC simulations from different starting configurations was explored, taking both ordered (cubic symmetry) and random initial configurations at each temperature. No statistically relevant differences emerged in the final HA and VI distributions, nor in the partial pair correlation functions obtained from these two initial configuration. The final configurations simulated from the random initial configurations are reported here. The shortest atom distances were determined from the experimentally measured total pair correlation function, $g(r)$. The number density trends linearly with temperature as

$$\rho(T) = -1.564 \cdot 10^{-6} \frac{T}{^{\circ}C \cdot Å^3} + .047 \frac{1}{Å^3}. \qquad (2)$$

Atomic models that are consistent with both the experimental scattering data and the MD simulations were obtained. The quality of the fit is shown in Fig. 2 for the $S(q)$ data taken at 978°C, 1090°C, 1217°C, and 1345°C. In all cases, a good fit was obtained at all scattering *q*. However, the intensities of the CRMC fit for the pre-peak and the primary peak are slightly higher than the experimental data, while the second peak, including the developing shoulder, was fit extremely well. The location of the pre-peak was also reproduced well. The discrepancy between the fit and experimental data for the pre-peak worsens slightly as the temperature is reduced, indicating that a quantitative analysis of the trends in ordering inherent to the second nearest neighbors is less reliable than for the nearest neighbors. .

*Figure 2 near here*

*Figure 3 near here*

Since RMC simulations provide average structures that fit the experimental data, poorly constrained RMC fits can produce partials with nonphysical peak positions. Lacking additional scattering data, MD partial pair-correlation functions are used to force the local atomic order to be consistent with both the experimental *S(q)* and the results of the MD simulation. The MD-derived partial pair-correlation functions provide realistic chemical interactions, at least to the first few shells [45]. MD data are often criticized for their small simulation size and short times. However, for liquid structure studies, where atomic mobility is high and typically atomic order does not extend beyond next-nearest neighbors, the MD results are expected to be accurate [47]. In Figure 3 we show the correspondence between the MD simulation partials and the CRMC partials at one temperature, 1345°C. The CRMC partials agree well with those obtained from the MD simulation. The small peak that is observed around 2.0Å in all of the partial pair correlation functions is nonphysical and appears to be a simulation artifact most likely due to a small difference between the number density for the experimental data and the simulations, and the finite resolution of the experimental data. A similar level of agreement is observed at all temperatures (not shown). With the constraints, the primary peak of the Zr-Pt partial (Fig. 3b) is near 2.80Å. It grows slightly with decreasing temperature, but doesn't sharpen or shift significantly. The location of the nearest neighbor peak is slightly smaller than would be expected from atomic size considerations alone, but is reasonable given the large negative heat of mixing between Zr and Pt (~100 kJ/mol[48]). The primary peak in the Zr-Zr partial *g(r)* is approximately 3.12Å, consistent with atomic size considerations. The peak sharpens and moves to lower *r* with decreasing temperature. The primary peak in the Pt-Pt partial is near 2.95Å. With decreasing temperature, the next-nearest neighbors (second peak in *g(r)*) split to form peaks at 4.50Å and 5.50Å. Interestingly, the intensity of the first peak *decreases* with decreasing temperature while the second peak *increases*; the intensity of the third peak remains relatively unchanged. All peak positions in the Pt-Pt pair correlation function remain unchanged over the temperature range studied.

The CRMC code assumes the Faber-Ziman formalism[49] for isotropic materials to construct the total pair correlation, $g(r)$ and structure factor, $S(q)$, from the experimental data. The partial pair correlations, $g_{i-j}(r)$, are calculated directly from the final atomic configurations

$$g_{i-j}(r) = \rho_{ij}^{-2} \left\langle \sum_i \sum_{j \neq k} \delta(\mathbf{r}_i) \delta(\mathbf{r} - \mathbf{r}_j) \right\rangle, \tag{3}$$

where $\rho_{ij}$ is the partial density,

$$\rho_{ij} = \rho_0 \sqrt{a_i a_j}\ , \tag{4}$$

$\rho_0$ is the average atomic density, and $a_i$ and $a_j$ are the atomic concentrations of the two species in the liquid. The partial structure factors, $S_{i-j}(q)$ and the partial pair correlation functions, $g_{i-j}(r)$, are related by a Fourier transform:

$$S_{i-j}(q) = 1 + 4\pi\rho_{ij} \int \left(g_{i-j}(r) - 1\right) \frac{\sin qr}{qr} r^2 dr \tag{5}$$

$$g_{i-j}(r) = 1 + \frac{1}{4\pi\rho_{ij}} \frac{2}{\pi} \int \left(S_{i-j}(q) - 1\right) \frac{\sin qr}{qr} q^2 dq\ . \tag{6}$$

The total $S(q)$ is obtained from the three partial structure factors, the X-ray atomic form factors, $f_i(q)$, and their atomic concentrations,

$$\begin{aligned} S(q) - 1 &= \frac{\sum_i \sum_j a_i a_j f_i(q) f_j(q) \left(S_{i-j}(q) - 1\right)}{\left(a_i f_i(q) + a_j f_j(q)\right)^2} \\ &\equiv S'_{Zr-Zr}(q) + S'_{Zr-Pt}(q) + S'_{Pt-Pt}(q) \end{aligned}\ . \tag{7}$$

Here, $S'_{i-j}(q)$, represent the properly weighted contributions from the three species-species contributions to the overall structure factor; they are shown in Fig 4. for all temperatures. Consistent with previous reports for the glass[15, 40, 50], the $S'_{i-j}(q)$ data indicate that the pre-peak S(q) data originates primarily from the Pt-Pt correlation.

*Figure 4 near here*

As noted earlier, the total structure factor (Fig. 4a) shows a developing shoulder on the high-q side of the second peak, which, as shown in Fig. 4c, is dominated by changes in Zr-Zr correlations. The second peak in the Zr-Pt partial structure factor (Fig. 4b) is symmetric and does not appear to contribute significantly to the shoulder in the total *S(q)*. A strong asymmetry is observed in the Zr-Pt partial structure, broadening on the high-*q* side indicating a relatively large distribution in the nearest neighbor bonding.

The results of an HA index analysis of the structures obtained from the CRMC fits to the data are shown in Fig. 5. All liquid structures are dominated by icosahedral (1551) and distorted icosahedral (1431+1541) order. While the amount of distorted icosahedral order decreases slightly with decreasing temperature, the amount of icosahedral order increases, causing the overall icosahedral-like order to slightly increase with undercooling. Additionally, there is a significant amount of body centered cubic (1661+1441) crystal-like order, which increases slightly with decreasing temperature, but little face centered cubic (1421) or hexagonal close packed (1422) order. The numbers of 1311, 1321, 1331 bond pairs, representing the rhombus symmetrical features of short-range order, show very modest decreases with decreasing temperature. The small increases in icosahedral and bcc order are consistent with observations in other Zr-based liquids,[9, 10, 40] although the amount of change reported there is generally larger than observed here. An examination of the 1551 index shows that the species-specific distribution of root-pairs (Zr-Zr, Zr-Pt, Pt-Pt) remains relatively unchanged for all temperatures studied.

*Figure 5 near here*

HA indices provide information about the local short-range order around two given atoms (the root pair). They do not, however, indicate whether complete clusters exist; Voronoi polyhedra analysis provides more complete information about the topological and chemical environment around central atoms. The Voronoi polyhedra are characterized by the number, *n*, of faces with the subscript of each *n* corresponding to the number of edges for that face. The number of faces, then, corresponds to the number of nearest neighbors and the geometry of those faces provide information about the local symmetry around the central atom; distinct polyhedra correspond to different sets of indices of the form $<n_3,n_4,n_5,n_6>$. Figure 6 shows the fraction of the most abundant Voronoi polyhedra detected in the RMC atomic structures. Consistent with previous Voronoi analyses of glasses of similar composition to the liquid studied here[40, 51], the most abundant Zr-centered clusters (Fig. 6a) are the 14 coordinated (<0,2,8,4>), 13 coordinated (<0,3,6,4>, <0,1,10,2>, <0,2,8,3>), and 12 coordinated (<0,3,6,3>, <0,2,8,2>) polyhedra. The numbers of all of these polyhedra increase slightly with decreasing temperature and the average coordination number around the Zr atoms changes from 12.75 to 13.05 over the temperature range, becoming largest at the lowest temperature. It should be noted that a Voronoi analysis of the local structure of the primary crystallizing phase, β-Zr (bcc) yields only <0,6,0,8> (truncated octahedrons) around the Zr atoms. This index is not a dominant feature in the RMC liquid structures.

*Figure 6a near here*

*Figure 6b near here*

While the HA analysis indicates that icosahedral and distorted icosahedral order are dominant in the liquid structure, the fraction of <0,0,12,0> Voronoi polyhedra (icosahedral clusters) is low. This is due partially to the failure of the HA analysis to identify complete clusters. Additionally, Hao *et al*[52] point out that distinct topological classes can be very closely related by simple distortions or coordination number increases. It can be shown that <0,2,8,2>, <0,1,10,2>, <0,4,4,4> and <0,2,8,4> , which are present in significant concentration, are closely related topologically to <0,0,12,0>. The Voronoi analysis, then, also demonstrates that the local structures of the atomic ensemble obtained by RMC have an icosahedral or distorted icosahedral character. The icosahedral order likely continues to increase during the quench, supported by the observation[12] that the quasicrystalline phase appears first upon devitrification of amorphous ribbons produced by rapid quenching, or in partially crystalline ribbons produced by slower quenching.

Based on high-energy X-ray scattering studies[15, 40, 51] and molecular dynamics (MD) simulations[40] of amorphous $Zr_{80}Pt_{20}$ and $Zr_{73}Pt_{27}$, the pre-peak in the structure factor has been attributed to Pt-Pt correlations. Further, Saida *et al*[51] and Wang *et al.*[40] found that the Pt-centered <0,2,8,1> cluster, which is a structural unit of the hexagonal primary crystallizing phase, $Zr_5Pt_3$ and which we find is a dominant structural unit in the liquid, is also dominant in the glass. Based on the CRMC simulation of the $Zr_{80}Pt_{20}$ liquid, the most dominant Pt-centered clusters (Fig. 6b) are the 13 coordinated (<0,3,6,4>), 12 coordinated (<0,2,8,2>, <0,3,6,3>, <0,4,4,4>), and 11 coordinated (<0,2,8,1>, <0,4,4,3>, <0,3,6,2>) polyhedra. The distribution of Pt-centered polyhedra shows no trend that exceeds the statistical noise, and the increase in the <0,2,8,2> index at 1090°C is likely not significant. The average coordination number around the Pt atoms remains constant, near 12.2, over the entire temperature range.

The persistence of the Pt-centered <0,2,8,1> polyhedra in the liquid and glassy Zr-Pt, and its existence in the $Zr_5Pt_3$ structure demonstrates the stability of this cluster. The large supercooling that is observed and glass formation indicate a significant nucleation barrier for $Zr_5Pt_3$. That the <0,2,8,1> polyhedra is observed in all phases seems to be inconsistent with this, although it should be emphasized that it is only one of the dominant clusters in the liquid (Fig. 6b). Glass formation and crystallization may be impacted by the chemical and other topological SRO and MRO in Zr-Pt liquids. $Zr_{80}Pt_{20}$ is known to form the i-phase directly from the melt while $Zr_{70}Pd_{30}$ does not,[12] suggesting that, in this system, the liquid that is richer in Zr contains more icosahedral order. Previous studies of Zr-Pt glasses support this, showing that the devitrification pathway changes with Zr concentration, going from $glass \Rightarrow Zr_5Pt_3$ at high Pt concentration to $glass \Rightarrow i\text{-}phase \Rightarrow Zr_5Pt_3$ with increasing Zr[53] and suggesting that icosahedral clusters are the source of the MRO observed. However, the recent observation of a pre-peak in a

Zr-Ni liquid[23] from neutron scattering data, which is reported not to have dominate icosahedral short-range order, suggests that icosahedral order isn't always the source of MRO. Instead, a pre-peak is a manifestation of chemical and topological ordering originating from the most common polyhedral cluster in each system—icosahedral or otherwise. This is further supported by the reports of pre-peaks in marginal Al-TM-RE glass forming alloys[26,54] and alkali metal alloys with Pb[55]. The pre-peak in a given system is enhanced (or reduced) depending on the atomic scattering factors and alloy composition; X-ray diffraction studies are insufficient to resolve this order in all cases.

## III. Conclusion

In summary, X-ray diffraction studies have revealed the existence of a pre-peak at $q \sim 1.7$ $Å^{-1}$ in the static structure factor of $Zr_{80}Pt_{20}$ equilibrium and supercooled liquids, indicating medium-range order in the liquid. An analysis of atomic structures obtained from a RMC fit, constrained by partials obtained from an MD simulation, to the scattering data indicates that the pre-peak is due to a Pt-Pt correlation among Zr-centered clusters having icosahedral/distorted-icosahedral symmetry. The icosahedral order in the liquid likely increases the crystal nucleation barrier, contributing to the ability to supercool and aiding glass formation in these alloys.

## Acknowledgements

We acknowledge the valuable assistance of D. Robinson, A. Logan, A. Lyons, J. Mai, and C. Tackes. The research was partially supported by the National Science Foundation under grants DMR-06-06065, DMR-08-56199, and DMR- 08157157, and NASA under grants NNX07AK27G and NNX09AJ19H. The synchrotron measurements were made on the MUCAT beam-line at the Advanced Photon Source. Work in the MUCAT Sector at the APS, and the Ames Laboratory was supported by the Department of Energy, Basic Energy Sciences, under Contract No. DS-AC02-07CH11358. Use of the Advanced Photon Source was supported by the U. S. Department of Energy, Office of Science, Office of Basic Energy Sciences, under Contract No. DE-AC02-06CH11357.

## References

1 T. Zhang, A. Inoue, and T. Masumoto, Mater. Trans., JIM **32**, 1005 (1991).
2 A. Peker and W. L. Johnson, Appl. Phys. Lett. **63**, 2342 (1993).
3 J. Saida, C. Li, M. Matsushita, and A. Inoue, J. Mat. Res. **76**, 55 (2001).
4 A. Inoue, T. Zhang, J. Saida, M. Matsushita, M. W. Chen, and T. Sakurai, Mater. Trans., JIM **40**, 1181 (1999).
5 J. Saida and A. Inoue, J. Phys. Condens. Matter **13**, L73 (2001).
6 L. Q. Xing, J. Eckert, W. Loeser, and L. Schultz, Appl. Phys. Lett. **74**, 664 (1999).
7 U. Koester, J. Meinhardt, S. Roos, and H. Liebertz, Appl. Phys. Lett. **69**, 179 (1996).

[8] K. F. Kelton, G. W. Lee, A. K. Gangopadhyay, R. W. Hyers, T. J. Rathz, J. R. Rogers, M. B. Robinson, and D. S. Robinson, Phys. Rev. Lett. **90**, 195504 (2003).
[9] K. F. Kelton, A. K. Gangopadhyay, T. H. Kim, and G. W. Lee, J. Non-Cryst. Solids **352**, 5318 (2006).
[10] Y. T. Shen, T. H. Kim, A. K. Gangopadhyay, and K. F. Kelton, Phys. Rev. Lett. **102**, 057801 (2009).
[11] M. J. Kramer, M. Xu, Y. Y. Ye, D. J. Sordelet, and J. R. Morris, Metall. Mater. Trans. A **39**, 1847 (2008).
[12] J. Saida, M. Matsushita, and A. Inoue, J. Appl. Phys. **90**, 4717 (2001).
[13] B. S. Murty, D. H. Ping, M. Ohnuma, and K. Hono, Acta Mat. **49**, 3453 (2001).
[14] M. Kitada, M. Imafuku, J. Saida, and A. Inoue, J. Non-Cryst. Solids **312-314**, 594 (2002).
[15] D. J. Sordelet, R. T. Ott, M. Z. Li, S. Y. Wang, C. Z. Want, M. F. Besser, A. C. Y. Liu, and M. J. Kramer, Metall. Mater. Trans. A **39A**, 1908 (2008).
[16] K. S. Bondi, A. K. Gangopadhyay, Z. Marine, T. H. Kim, A. Mukhopadhyay, A. I. Goldman, W. E. Buhro, and K. F. Kelton, J. Non-Cryst. Solids **353**, 4723 (2007).
[17] W. Hoyer and R. Jödicke, J. Non-Cryst. Solids **192-193**, 102 (1995).
[18] L. Wang, Y. Wang, C. Peng, and Y. Zhang, Phys. Lett. A **350**, 405 (2006).
[19] T. Nakamura, E. Matsubara, M. Sakurai, M. Kasai, A. Inoue, and Y. Waseda, J. Non-Cryst. Solids **312-314**, 517 (2002).
[20] X. Hui, R. Gao, G. L. Chen, S. L. Shang, Y. Wang, and Z. K. Liu, Phys. Lett. A **372**, 3078 (2008).
[21] M. Wakeda and Y. Shibutani, Acta Mat. **In Press, Corrected Proof**.
[22] X. Bian, M. Sun, X. Xue, and X. Qin, Materials Letters **57**, 2001 (2003).
[23] D. Holland-Moritz, St, uuml, S. ber, H. Hartmann, T. Unruh, T. Hansen, and A. Meyer, Phys. Rev. B **79**, 064204 (2009).
[24] I. Kaban, W. Hoyer, A. Il'inskii, A. Shpak, and P. Jóvári, J. Non-Cryst. Solids **353**, 1808 (2007).
[25] L. Wang, H. Cong, and X. Bian, Mater. Sci. Eng. **341**, 197 (2003).
[26] L. Zhang, Y. Wu, X. Bian, H. Li, W. Wang, and S. Wu, J. Non-Cryst. Solids **262**, 169 (2000).
[27] J. Brillo, A. Bytchkov, I. Egry, L. Hennet, G. Mathiak, I. Pozdnyakova, D. L. Price, D. Thiaudiere, and D. Zanghi, J. Non-Cryst. Solids **352**, 4008 (2006).
[28] A. K. Gangopadhyay, G. W. Lee, K. F. Kelton, J. R. Rogers, A. I. Goldman, D. S. Robinson, T. J. Rathz, and R. W. Hyers, Rev. Sci. Instrum. **76**, 073901 (2005).
[29] N. A. Mauro and K. F. Kelton, in *Rev. Sci. Instrum.*, 2010.
[30] T. Meister, H. Werner, G. Lohoefer, D. M. Herlach, and H. Unbehauen, Cont. Engin. Pract. **11**, 117 (2003).
[31] S. K. Chung, D. B. Thiessen, and W.-K. Rhim, Rev. Sci. Instrum. **67**, 3175 (1996).
[32] R. C. Bradshaw, J. R. Rogers, K. F. Kelton, R. W. Hyers, and D. P. Schmidt, Rev. Sci. Instrum. **76**, 125108 (2005).
[33] A. P. Hammersley, in *ESRF Internal Report, ESRF97HA02T*, 1997).
[34] I. K. Jeong, J. Thompson, T. Proffen, A. M. P. Turner, and S. J. Billinge, J. Appl. Crys. **34**, 536 (2001).

[35] G. Gresse and J. Hafner, Phys. Rev. B **47**, 558 (1993).
[36] G. Kresse, Technische Universität Wien, 1993.
[37] G. Kresse and J. Furthmüller, Computational Material Science **6**, 15 (1996).
[38] G. Kresse and J. Furthmüller, Phys. Rev. B **54**, 11169 (1996).
[39] G. Kresse and D. Joubert, Phys. Rev. B **59**, 1758 (1999).
[40] S. Y. Wang, C. Z. Wang, M. Z. Li, L. Huang, R. T. Ott, M. J. Kramer, D. J. Sordelet, and K. M. Ho, Phys. Rev. B **78**, 184204 (2008).
[41] T. H. Kim and K. F. Kelton, J. Chem. Phys. **126**, 054513 (2007).
[42] M. L. McGreevy, J. Phys. Condens. Matter **3**, F9 (1991).
[43] D. A. Keen, Nature (London) **344**, 423 (1990).
[44] J. D. Honeycutt and H. C. Andersen, J Phys. Chem. **91**, 4950 (1987).
[45] J. L. Finney, Nature (London) **266**, 309 (1977).
[46] J. L. Finney, Proc. Roy. Soc. London A **319**, 479 (1970).
[47] H. Okamoto, J. Phase Equil. and Diff. **29**, 385 (2008).
[48] F. R. D. Boer, R. Boom, W. C. M. Mattens, A. R. Miedema, and A. K. Niessen, *Cohesion In Metals: Transition Metal Alloys (Cohesion And Structure)* (Elsevier Science Ltd, 1989).
[49] T. E. Faber and J. M. Ziman, Philos. Mag. **11**, 153 (1965).
[50] J. Saida, T. Sanada, S. Sato, M. Imafuku, and A. Inoue, Appl. Phys. Lett. **91**, 111901 (2007).
[51] J. Saida, K. Itoh, S. Sato, M. Imafuku, T. Sanada, and A. Inoue, J. Phys. Condens. Matter **21**, 375104 (2009).
[52] S. G. Hao, C. Z. Wang, M. J. Kramer, and K. M. Ho, J. Appl. Phys. **107**, 053511 (2010).
[53] M. H. Lee, R. T. Ott, M. F. Besser, M. J. Kramer, and D. J. Sordelet, Scr. Mater **55**, 737 (2006).
[54] K. Saksl, P. Jovari, H. Franz, and J. Z. Jiang, J. Appl. Phys. **97**, 113507 (2005).
[55] H. T. J. Reijers, M. L. Saboungi, D. L. Price, J. W. Richardson, K. J. Volin, and W. van der Lugt, Phys. Rev. B **40**, 6018 (1989).

## *Figure Captions*

**Figure 1** - Static structure factor, *S(q)* for a.) liquid $Zr_{80}Pt_{20}$ at 1607°C, 1474°C, 1345°C, 1217°C, 1090°C, and 978°C. The inserts show the evolution of *S(q)* with decreasing temperature for b.) the primary peak, c.) the second peak and d.) the pre-peak (indicated with an arrow in the total structure factor).

**Figure 2** - Experimental *S(q)* (solid lines) and the corresponding CRMC fit (dashed lines) for liquid $Zr_{80}Pt_{20}$ at 1345°C, 1217°C, 1090°C, and 978°C.

**Figure 3** – (a) Structure factor *S(q)* of $Zr_{80}Pt_{20}$ liquid at 1345°C with the constrained RMC fit. Partial pair-correlation functions $g_{i-j}(r)$ from MD and CRMC simulations for (b) Zr-Pt, (c) Zr-Zr, and (d) Pt-Pt.

**Figure 4 –** *S(q)* produced from CRMC simulations at all temperatures. a.) Total Structure factor; b.) Zr-Pt partial structure factor, showing an asymmetric first peak and no developing shoulder in the second peak; c.) Zr-Zr partial structure factor showing a developing should in the second peak; d.) Pt-Pt partial structure factor displaying a prominent pre-peak at all temperatures.

**Figure 5** – The prominent HA indices for the RMC liquid structure as a function of temperature.

**Figure 6a** – Dominant Zr-centered Voronoi polyhedra as a function of temperature.

**Figure 6b -** Dominant Pt-centered Voronoi polyhedra as a function of temperature.

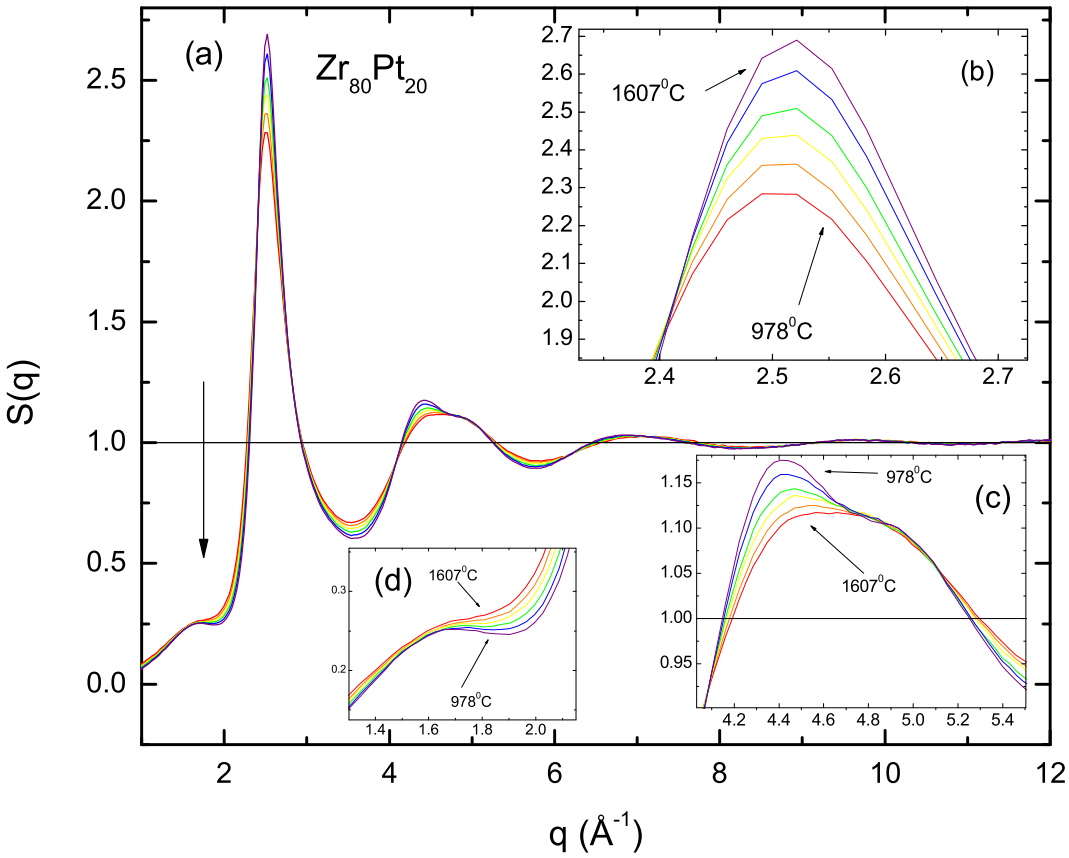


Figure 1 BW11124 17MAR2011

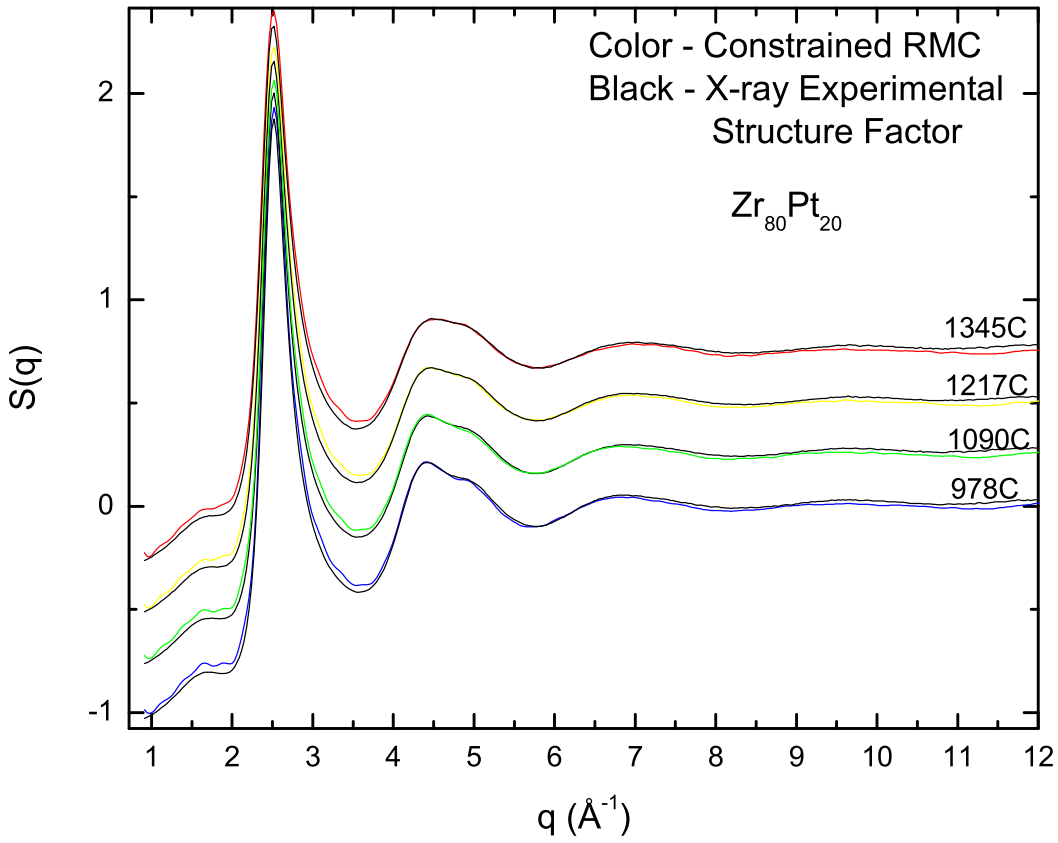


Figure 2 BW11124 17MAR2011

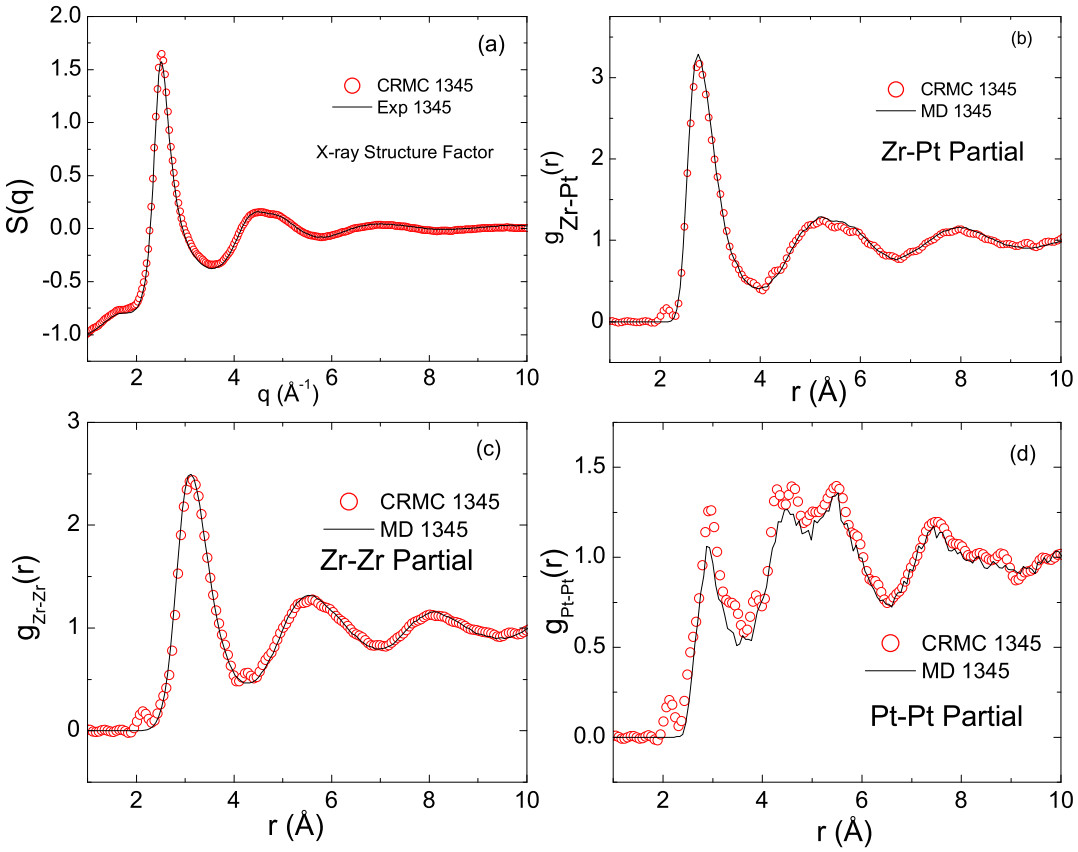


Figure 3 BW11124 17MAR2011

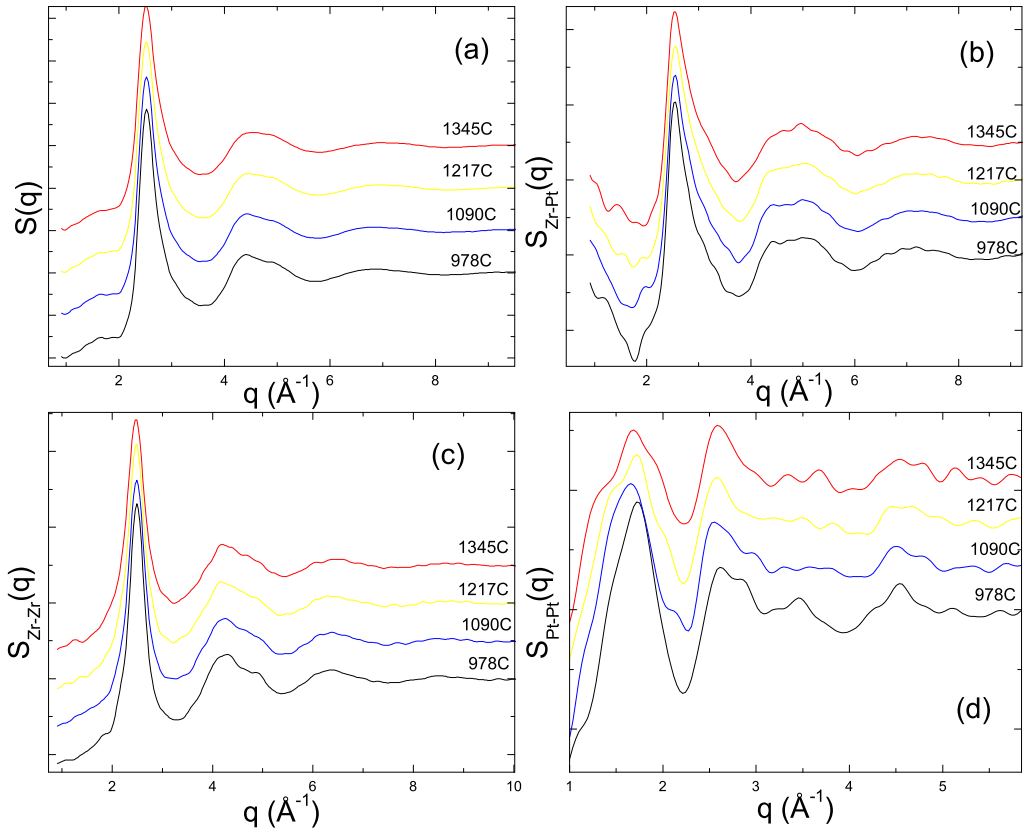


Figure 4 BW11124 17MAR2011

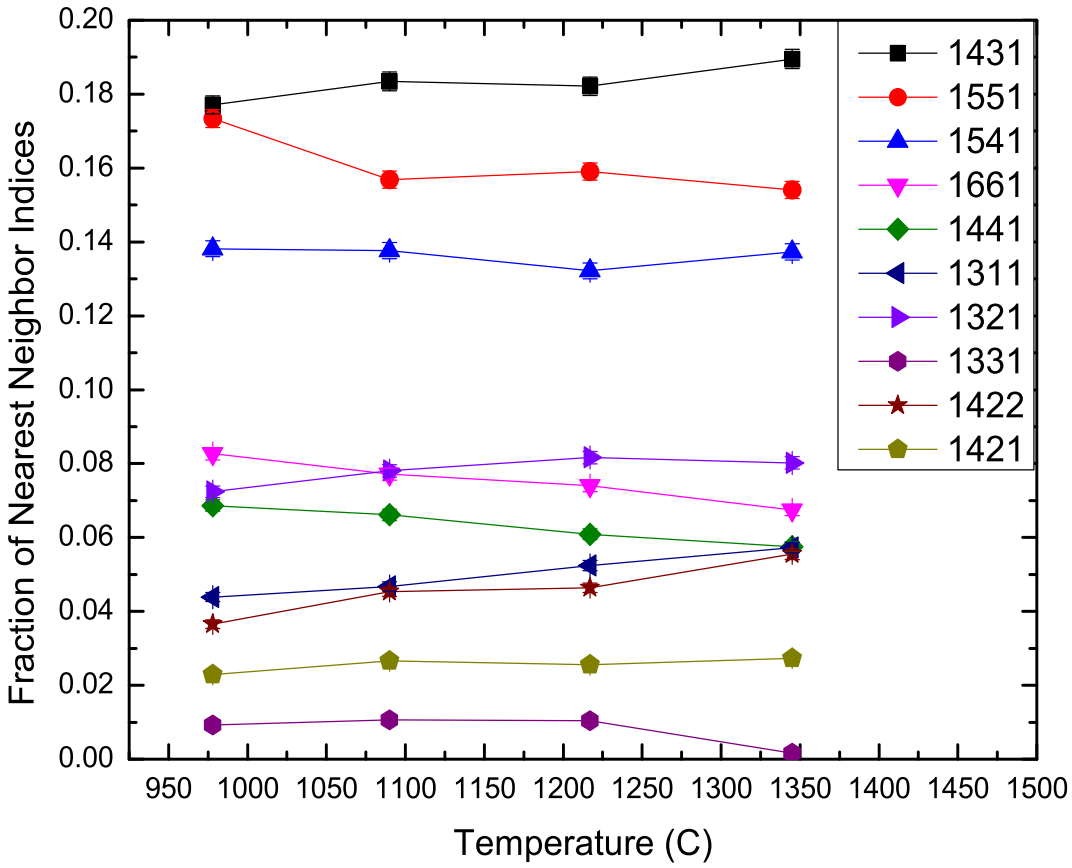


Figure 5 BW11124 17MAR2011

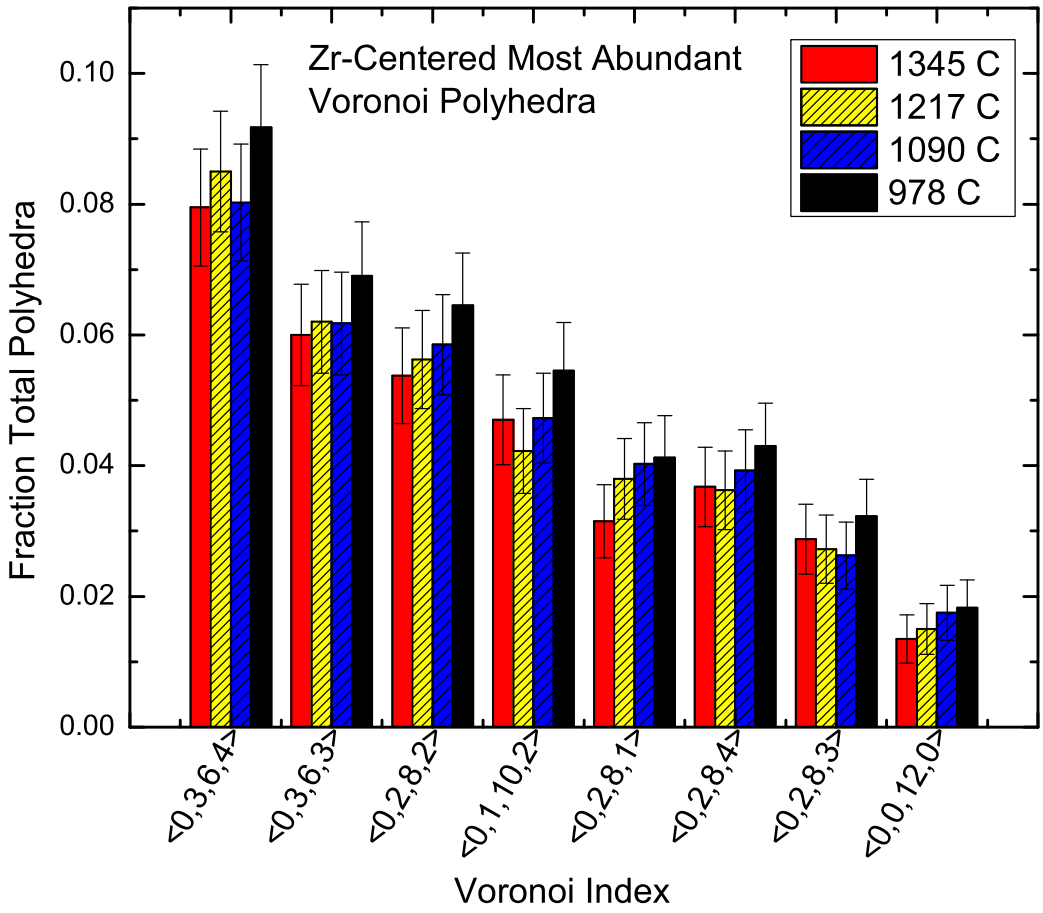


Figure 6a BW11124 17MAR2011

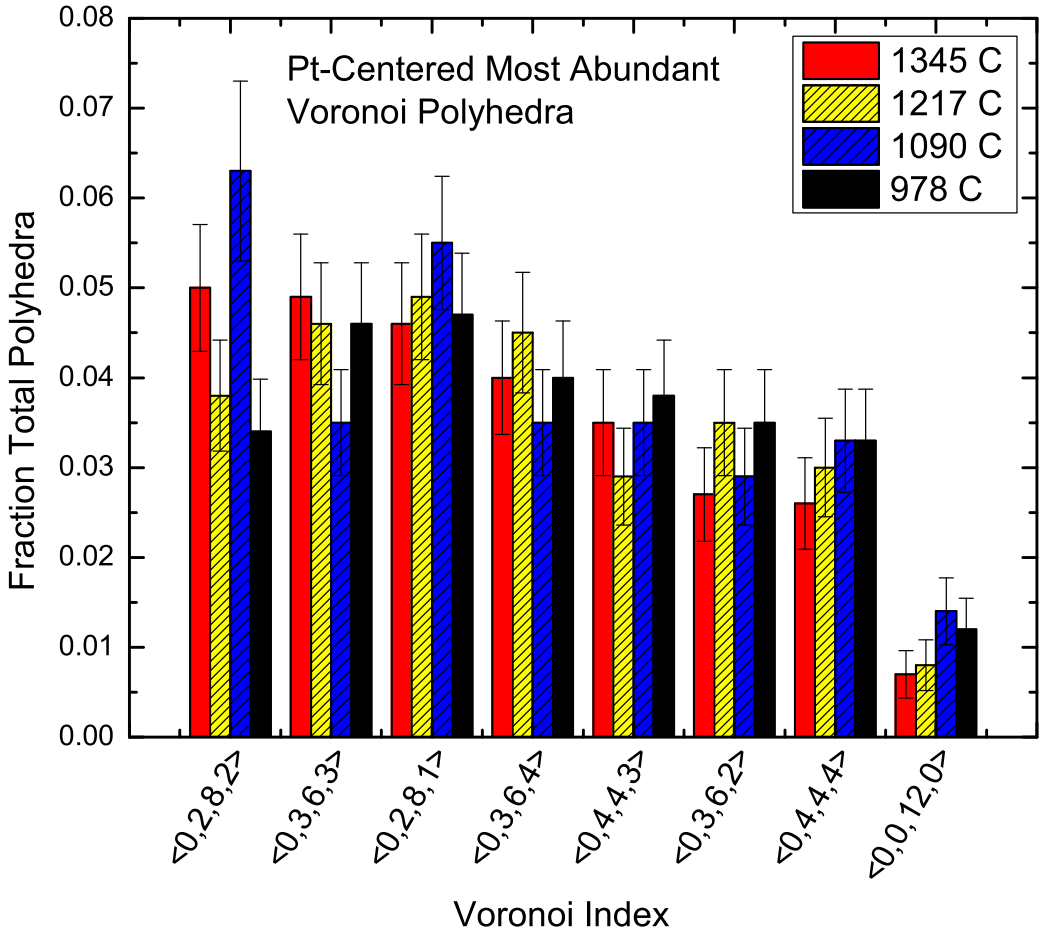


Figure 6b BW11124 17MAR2011